ACADEMIC PRESS

Available online at www.sciencedirect.com

SCIENCE DIRECT®

Journal of Sound and Vibration 264 (2003) 203–224

JOURNAL OF SOUND AND VIBRATION

www.elsevier.com/locate/jsvi

Power flow model of flexural waves in finite orthotropic plates

D.-H. Park[a], S.-Y. Hong[a,*], H.-G. Kil[b]

[a] *Department of Naval Architecture and Ocean Engineering, Seoul National University, San 56-1, Sillim-dong Kwanak-gu, Seoul 151-742, South Korea*

[b] *Department of Mechanical Engineering, The University of Suwon, Suwon 445-743, South Korea*

Received 27 February 2002; accepted 9 September 2002

Abstract

In this paper, an approximate power flow model is developed for the analysis of the flexural waves in finite orthotropic plate transversely vibrating in the medium-to-high frequency ranges. The derived energy equation for the model is expressed with time- and locally space-averaged farfield wave energy density. It could be the more general form than that of the conventional power flow analysis model seen in the isotropic plate. With the derived model, dynamic characteristics varying with the direction can be expressed. To verify the validity and accuracy of the model, numerical analyses are performed for the case where a finite rectangular plate is excited by a harmonic point force, and the calculated results expressed with the energy levels are compared with classical modal solutions by changing the frequency and the damping loss factor of the plate. The dominant power transmission paths in the plate are also predicted from the distribution of the approximate intensity fields.

© 2002 Elsevier Science Ltd. All rights reserved.

1. Introduction

The power flow analysis (PFA) method has been developed as a promising vibro-acoustic prediction tool of medium-to-high frequency ranges for recent decades. It has been generally noted that the PFA method offers an improved solution to the statistical energy analysis (SEA) that does not give the information on the energy variation in a subsystem and it is impossible to consider the local power input and damping treatment. The PFA model, analogous to the steady state heat flow model, was introduced by Belov et al. [1]. Nefske and Sung [2] applied power flow finite element method (PFFEM) for predicting the flexural vibration of beams. Further studies on PFA for rods and beams were performed by Wohlever and Bernhard [3–5]. Bouthier and

*Corresponding author. Tel.: +82-2-880-8757; fax: +82-2-888-9298.
E-mail address: syhong@gong.snu.ac.kr (S.-Y. Hong).

0022-460X/03/$ - see front matter © 2002 Elsevier Science Ltd. All rights reserved.
doi:10.1016/S0022-460X(02)01296-8

Bernhard [4–7] developed approximate power flow models for the propagation of the flexural waves in isotropic thin plates and membranes, and Park et al. [8] derived energy equations for the in-plane waves in isotropic thin plates.

Most of the dynamic complex structures such as ships and planes include the plates made of orthotropic materials and the stiffened or reinforced plates [9–11]. These naturally and structurally orthotropic plates have different bending stiffnesses in two perpendicular directions, on which the energy distribution and the power transmission path may greatly depend on certain conditions. Until recently, the development of the power flow models for the PFA method has been mainly focused on isotropic structural elements. Thus, more general power flow formulations are required for proper application of the PFA method to orthotropic structural elements.

The aim of this work is to develop an approximate power flow model that can be utilized to predict the distribution of energy and the power transmission path of the orthotropic plates vibrating in the medium-to-high frequency ranges in a time- and locally space-averaged sense. Numerical analyses are performed for a finite rectangular orthotropic plate simply supported along the edges and excited by a transverse harmonic point force located in the middle of the plate. The results obtained from the derived PFA model are compared with those from classical theory on orthotropic plates, and the effects of the frequency and damping are investigated.

2. Approximate power flow model for the transverse vibration of finite orthotropic plates

The equation of motion of thin orthotropic plates excited by a harmonic point force located at (x_0, y_0) of which the amplitude and the frequency are F and ω, respectively, can be written as [9,11]

$$D_{xc}\frac{\partial^4 w}{\partial x^4} + 2H_c\frac{\partial^4 w}{\partial x^2 \partial y^2} + D_{yc}\frac{\partial^4 w}{\partial y^4} + m\frac{\partial^2 w}{\partial t^2} = F\delta(x - x_o)\delta(y - y_o)e^{j\omega t}, \tag{1}$$

where w is the transverse displacement and m is the mass per unit area of the plate. D_{xc} and D_{yc} are the complex bending stiffnesses in the x and y directions, respectively, and are written as

$$D_{xc} = D_x(1 + j\eta) \quad \text{and} \quad D_{yc} = D_y(1 + j\eta), \tag{2}$$

where η is the hysteretic damping loss factor. H_c in Eq. (1) is the complex effective torsional stiffness. When the thickness of the plate is constant, the transverse displacement relatively very small and the deformation properly elastic, the effective torsional stiffness, H_c, can be assumed to be the geometric mean value of the bending stiffnesses D_{xc} and D_{yc}, as shown in the following expression [9]:

$$H_c = \sqrt{D_{xc}D_{yc}}. \tag{3}$$

The effective torsional stiffness expressed by Eq. (3) makes it easy to mathematically handle the equation of motion given by Eq. (1). Cremer and Heckl showed that Eq. (3) is a very good approximation for many practical orthotropic plates [12]. Substituting Eq. (3) into Eq. (1), the

equation of motion can be rewritten as

$$D_{xc}\frac{\partial^4 w}{\partial x^4} + 2\sqrt{D_{xc}D_{yc}}\frac{\partial^4 w}{\partial x^2 \partial y^2} + D_{yc}\frac{\partial^4 w}{\partial y^4} + m\frac{\partial^2 w}{\partial t^2} = F\delta(x - x_o)\delta(y - y_o)e^{j\omega t}, \tag{4}$$

from which an approximate power flow model of the orthotropic plates is investigated.

Eq. (4) has both far and nearfield solutions. It was shown by Noiseux [13] that the farfield solution is useful for the PFA of vibrating plates. The energy model for isotropic plates derived by Bouthier and Bernhard [4,6] was obtained with the farfield solution of the equation of motion and appeared to be good representation of the approximate response of the plates. Thus, as in the Bouthier's works, only the farfield solutions are utilized in this work for relevant analyses. When considering plane waves, the general form of the farfield solution can be expressed as the sum of the plane progressive wave components:

$$w_{ff}(x, y, t) = \left(Ae^{-j(k_x x + k_y y)} + Be^{j(k_x x - k_y y)} + Ce^{-j(k_x x - k_y y)} + De^{j(k_x x + k_y y)}\right)e^{j\omega t}, \tag{5}$$

where the unknown constants, A, B, C and D, are the amplitudes of the corresponding wave components. k_x and k_y are the complex wave numbers in the x and y directions, respectively. When k_{xl} and k_{yl} are real parts of k_x and k_y , the dispersion relation can be expressed as

$$\left(\sqrt{D_x}k_{xl}^2 + \sqrt{D_y}k_{yl}^2\right)^2 = \omega^2 m. \tag{6}$$

If the damping is small, k_x and k_y are well approximated by

$$k_x = k_{xl}\left(1 - j\frac{\eta}{4}\right) \quad \text{and} \quad k_y = k_{yl}\left(1 - j\frac{\eta}{4}\right). \tag{7}$$

In general, the vibrational energy in the plates is transmitted by shear forces, bending moments and twisting moments. The shear forces Q_{xz} and Q_{yz} of the orthotropic plate with the effective torsional stiffness $H = (D_x D_y)^{1/2}$ are expressed by the transverse displacement as

$$Q_{xz} = -\left(D_{xc}\frac{\partial^3 w}{\partial x^3} + \sqrt{D_{xc}D_{yc}}\frac{\partial^3 w}{\partial x \partial y^2}\right) \tag{8}$$

and

$$Q_{yz} = -\left(D_{yc}\frac{\partial^3 w}{\partial y^3} + \sqrt{D_{xc}D_{yc}}\frac{\partial^3 w}{\partial x^2 \partial y}\right), \tag{9}$$

respectively. The bending moments, M_x and M_y, are also written as

$$M_x = -D_{xc}\left(\frac{\partial^2 w}{\partial x^2} + v_y\frac{\partial^2 w}{\partial y^2}\right) \tag{10}$$

and

$$M_y = -D_{yc}\left(\frac{\partial^2 w}{\partial y^2} + v_x\frac{\partial^2 w}{\partial x^2}\right), \tag{11}$$

respectively, where v_x and v_y are the effective Poisson ratios of the orthotropic plate in the x and y directions, respectively. The twisting moment of the plates, M_{xy} ($M_{yx} = M_{xy}$) are written as

$$M_{xy} = -\left(1 - \sqrt{v_x v_y}\right)\sqrt{D_{xc}D_{yc}}\frac{\partial^2 w}{\partial x \partial y}. \tag{12}$$

The total energy density is the sum of the kinetic and potential energy densities. With the above equations (8)–(12), the time-averaged total energy density of the orthotropic plate can be expressed as

$$\begin{aligned}\langle e\rangle = &\frac{1}{4}\,\mathrm{Re}\left\{ D_{xc}\frac{\partial^2 w}{\partial x^2}\left(\frac{\partial^2 w}{\partial x^2}\right)^* + 2\sqrt{v_x v_y}\sqrt{D_{xc}D_{yc}}\frac{\partial^2 w}{\partial x^2}\left(\frac{\partial^2 w}{\partial y^2}\right)^* \right.\\ &\left. + D_{yc}\frac{\partial^2 w}{\partial y^2}\left(\frac{\partial^2 w}{\partial y^2}\right)^* + 2\left(1 - \sqrt{v_x v_y}\right)\sqrt{D_{xc}D_{yc}}\frac{\partial^2 w}{\partial x \partial y}\left(\frac{\partial^2 w}{\partial x \partial y}\right)^* + m\frac{\partial w}{\partial t}\left(\frac{\partial w}{\partial t}\right)^* \right\},\end{aligned} \tag{13}$$

where Re{ } represents the real part. The bracket $\langle\rangle$ means the time average over one period, and the superscript * indicates the complex conjugate. The x and y components of the time-averaged intensity $\langle \mathbf{q}\rangle$ of a vibrating orthotropic plate are expressed by the shear forces, bending moments, twisting moments and the transverse displacement, as follows:

$$\langle q_x\rangle = \frac{1}{2}\,\mathrm{Re}\left\{ -Q_{xz}\left(\frac{\partial w}{\partial t}\right)^* + M_x\left(\frac{\partial^2 w}{\partial x \partial t}\right)^* + M_{xy}\left(\frac{\partial^2 w}{\partial y \partial t}\right)^* \right\} \tag{14}$$

and

$$\langle q_y\rangle = \frac{1}{2}\mathrm{Re}\left\{ -Q_{yz}\left(\frac{\partial w}{\partial t}\right)^* + M_y\left(\frac{\partial^2 w}{\partial y \partial t}\right)^* + M_{yx}\left(\frac{\partial^2 w}{\partial x \partial t}\right)^* \right\}, \tag{15}$$

respectively. The farfield energy density can be obtained by substituting Eq. (5) into Eq. (12). The expression for the time-averaged farfield energy density expanded in terms of the constants $A, \ldots, D$ in Eq. (5) becomes

$$\begin{aligned}\langle e\rangle = &\tfrac{1}{4}\,\mathrm{Re}\Big\{ D_{xc}|k_x|^4\left|[A]^{--} + [B]^{+-} + [C]^{-+} + [D]^{++}\right|^2\\ &+ 2\sqrt{v_x v_y}\sqrt{D_{xc}D_{yc}}k_x^2\left(k_y^2\right)^*\left|[A]^{--} + [B]^{+-} + [C]^{-+} + [D]^{++}\right|^2\\ &+ 2\left(1 - \sqrt{v_x v_y}\right)\sqrt{D_{xc}D_{yc}}|k_x|^2|k_y|^2\left|[A]^{--} - [B]^{+-} - [C]^{-+} + [D]^{++}\right|^2\\ &+ D_{yc}|k_y|^4\left|[A]^{--} + [B]^{+-} + [C]^{-+} + [D]^{++}\right|^2\\ &+ m\omega^2\left|[A]^{--} + [B]^{+-} + [C]^{-+} + [D]^{++}\right|^2\Big\},\end{aligned} \tag{16}$$

where $[\ ]^{\pm\pm}$ means $[\ ]\times\ \exp(\pm \mathrm{j}k_x x \pm \mathrm{j}k_y y)$. The x and y components of the farfield intensity can be obtained by substituting Eq. (5) into Eqs. (14) and (15). The expanded expressions for the

time-averaged farfield intensity components are written as

$$\begin{aligned}\langle q_x\rangle = &\frac{\omega}{2}\,\mathrm{Re}\Big\{k_x\Big(D_{xc}k_x^2+\sqrt{D_{xc}D_{yc}}k_y^2\Big)\\ &\times\big([A]^{--}-[B]^{+-}+[C]^{-+}-[D]^{++}\big)\big([A]^{--}+[B]^{+-}+[C]^{-+}+[D]^{++}\big)^*\\ &+D_{xc}\Big(k_x^2+v_yk_y^2\Big)k_x^*\\ &\times\big([A]^{--}+[B]^{+-}+[C]^{-+}+[D]^{++}\big)\big([A]^{--}-[B]^{+-}+[C]^{-+}-[D]^{++}\big)^*\\ &+\Big(1-\sqrt{v_xv_y}\Big)\sqrt{D_{xc}D_{yc}}k_x|k_y|^2\\ &\times\big([A]^{--}-[B]^{+-}-[C]^{-+}+[D]^{++}\big)\big([A]^{--}+[B]^{+-}-[C]^{-+}-[D]^{++}\big)^*\Big\}\end{aligned}\tag{17}$$

and

$$\begin{aligned}\langle q_y\rangle = &\frac{\omega}{2}\mathrm{Re}\Big\{k_y\Big(D_{yc}k_y^2+\sqrt{D_{xc}D_{yc}}k_x^2\Big)\\ &\times\big([A]^{--}+[B]^{+-}-[C]^{-+}-[D]^{++}\big)\big([A]^{--}+[B]^{+-}+[C]^{-+}+[D]^{++}\big)^*\\ &+D_{yc}\Big(k_y^2+v_xk_x^2\Big)k_y^*\\ &\times\big([A]^{--}+[B]^{+-}+[C]^{-+}+[D]^{++}\big)\big([A]^{--}+[B]^{+-}-[C]^{-+}-[D]^{++}\big)^*\\ &+\Big(1-\sqrt{v_xv_y}\Big)\sqrt{D_{xc}D_{yc}}|k_x|^2k_y\\ &\times\big([A]^{--}-[B]^{+-}-[C]^{-+}+[D]^{++}\big)\big([A]^{--}-[B]^{+-}+[C]^{-+}-[D]^{++}\big)^*\Big\}\end{aligned}\tag{18}$$

Eqs. (16)–(18) consist of purely exponentially decayed terms (i.e., $|[A]^{--}|^2, \ldots, \left|[D]^{++}\right|^2$) and spatially harmonic terms (i.e., $[A]^{--}([B]^{+-})^*$, $[C]^{-+}([B]^{+-})^*$). At this stage, no obvious relations between the energy density (Eq. (16)) and the intensity components (Eqs. (17) and (18)) can be found. Thus, the time-averaged farfield energy density and intensity are spatially averaged over a half wavelength for small damping in the following manner [6,8]:

$$\langle\tilde{e}\rangle=\frac{k_{xl}k_{yl}}{\pi^2}\int_0^{\pi/k_{yl}}\int_0^{\pi/k_{xl}}\langle e\rangle\,\mathrm{d}x\,\mathrm{d}y\tag{19}$$

and

$$\langle\tilde{\mathbf{q}}\rangle=\frac{k_{xl}k_{yl}}{\pi^2}\int_0^{\pi/k_{yl}}\int_0^{\pi/k_{xl}}\langle\mathbf{q}\rangle\,\mathrm{d}x\,\mathrm{d}y,\tag{20}$$

respectively, where $\langle\tilde{e}\rangle$ and $\langle\tilde{\mathbf{q}}\rangle$ are the time- and space-averaged energy density and intensity, respectively. The space-averaging process removes the interference of different wave components and thus, the spatially harmonic terms in Eqs. (16)–(18) can be neglected by the above equations (19) and (20). Moreover, neglecting all of the second and higher order terms of the damping loss factor, which is small, yields a simplified expression for the energy density as

follows (Appendix B):

$$\langle \tilde{e} \rangle = \tfrac{1}{2}\omega^2 m\left(|A|^2 e^{--} + |B|^2 e^{+-} + |C|^2 e^{-+} + |D|^2 e^{++}\right), \tag{21}$$

where $e^{\pm\pm}$ means $\exp\{\pm(\eta/2)k_{xl}x \pm (\eta/2)k_{yl}y\}$. It can be noted in Eq. (21) that the total farfield wave energy density may be represented as the linear combination of the energy densities of four plane wave components when the damping is small and the wave interferences are neglected. The simplified expressions for the x and y components of the time- and space-averaged intensity are written as

$$\langle \tilde{q}_x \rangle = \omega k_{xl}\sqrt{D_x}\sqrt{\omega^2 m}\left(|A|^2 e^{--} - |B|^2 e^{+-} + |C|^2 e^{-+} - |D|^2 e^{++}\right) \tag{22}$$

and

$$\langle \tilde{q}_y \rangle = \omega k_{yl}\sqrt{D_y}\sqrt{\omega^2 m}\left(|A|^2 e^{--} + |B|^2 e^{+-} - |C|^2 e^{-+} + |D|^2 e^{++}\right) \tag{23}$$

respectively. In Eqs. (22) and (23), the net intensity is represented as the subtraction of the intensities of the waves propagating in the negative direction from those of the waves propagating in the positive direction. From Eqs. (21)–(23) and the dispersion relation (Eq. (6)), it can be easily found that the x and y components of the time- and locally space-averaged intensity of the farfield wave are proportional to the first derivatives of the time- and locally space-averaged farfield wave energy density with respect to x and y, as follows:

$$\langle \tilde{q}_x \rangle = -\frac{4}{\eta\omega}\sqrt{\frac{\omega^2 D_x}{m}}\,\frac{\partial\langle \tilde{e} \rangle}{\partial x} \tag{24}$$

and

$$\langle \tilde{q}_y \rangle = -\frac{4}{\eta\omega}\sqrt{\frac{\omega^2 D_y}{m}}\,\frac{\partial\langle \tilde{e} \rangle}{\partial y}, \tag{25}$$

respectively. Consequently, rearranging Eqs. (24) and (25) into a vector form, the intensity can be rewritten as

$$\langle \tilde{\mathbf{q}} \rangle = -\left(\frac{c_{gx}^2}{\eta\omega}\frac{\partial}{\partial x}\mathbf{i} + \frac{c_{gy}^2}{\eta\omega}\frac{\partial}{\partial y}\mathbf{j}\right)\langle \tilde{e} \rangle, \tag{26}$$

where c_{gx} and c_{gy} are defined here as follows:

$$c_{gx} = 2\left(\frac{\omega^2 D_x}{m}\right)^{1/4} \quad \text{and} \quad c_{gy} = 2\left(\frac{\omega^2 D_y}{m}\right)^{1/4}, \tag{27}$$

respectively. Eq. (26) is the expression for the vibrational energy transmission, in which the dynamic characteristics of the orthotropic plates is sustained due to the different values of c_{gx} and c_{gy}.

The power injected by external loads into an elastic medium is dissipated due to the damping and is transmitted to the next media. For the steady state elastic system, the power balance

equation can be written as

$$\nabla \cdot \mathbf{q} + \pi_{diss} = \pi_{in}, \tag{28}$$

where π_{diss} and π_{in} are the dissipated power due to the damping of the system and the input power, respectively. From the work of Cremer and Heckl [12], the time-averaged dissipated power in an elastic medium with small structural damping is proportional to the time-averaged total energy density in the form

$$\langle \pi_{diss} \rangle = \eta\omega \langle e \rangle, \tag{29}$$

where it is assumed that the kinetic and potential energies of the medium are approximately the same. Combination of the power balance equation (Eq. (28)) with the energy transmission relation (Eq. (26)) and the power dissipation relation (Eq. (29)) yields the second order partial differential equation that takes the total energy density as a primary variable:

$$-\left(\frac{c_{gx}^2}{\eta\omega}\frac{\partial^2}{\partial x^2} + \frac{c_{gy}^2}{\eta\omega}\frac{\partial^2}{\partial y^2}\right)\langle \tilde{e} \rangle + \eta\omega \langle \tilde{e} \rangle = \langle \tilde{\pi}_{in} \rangle. \tag{30}$$

Eq. (30) is a power flow model expressed with the time- and space-averaged energy density for the farfield flexural waves in orthotropic plates.

If both the bending stiffnesses D_x and D_y of the plate are assumed to be equal to the bending stiffness D of an isotropic plate, c_{gx} and c_{gy} then become

$$c_{gx} = c_{gy} = c_g = 2\left(\frac{\omega^2 D}{m}\right)^{1/4}, \tag{31}$$

where c_g is the group velocity of the corresponding isotropic plate. In this particular case, the energy equation is deduced from Eq. (30) as follows:

$$-\frac{c_g^2}{\eta\omega}\left(\frac{\partial^2}{\partial x^2} + \frac{\partial^2}{\partial y^2}\right)\langle \tilde{e} \rangle + \eta\omega \langle \tilde{e} \rangle = \langle \tilde{\pi}_{in} \rangle \tag{32}$$

where $\langle \tilde{e} \rangle$ is the time- and space-averaged total energy density of the farfield waves in isotropic thin plates. It can be known that Eq. (32) is the same as the energy equation developed by Bouthier and Bernhard [6–9] for the farfield flexural waves in isotropic thin plates.

3. Power flow analysis of a rectangular orthotropic plate

3.1. Approximate solution of energy equation

In this section, the energy equation derived in the previous section is applied to the finite rectangular orthotropic plate simply supported along its edges and excited by a transverse point force at a single frequency. When the exciting force is located at (x_0, y_0) in the plate, Eq. (30) becomes

$$-\left(\frac{c_{gx}^2}{\eta\omega}\frac{\partial^2}{\partial x^2} + \frac{c_{gy}^2}{\eta\omega}\frac{\partial^2}{\partial y^2}\right)\langle \tilde{e} \rangle + \eta\omega \langle \tilde{e} \rangle = \Pi_{in}\delta(x - x_o)\delta(y - y_o), \tag{33}$$

where Π_{in} is the time-averaged input power due to the exciting force and δ is the Dirac delta. When the plate is simply supported, free or fixed at its boundary, it can be assumed that there is no outflow of power from the boundary, and thus the energy density solution of Eq. (34) can be expressed by the double Fourier series of the cosine functions with respect to the spatial variables x and y [5,14]:

$$\langle \tilde{e} \rangle = \sum_{m=0}^{\infty} \sum_{n=0}^{\infty} E_{mn} \cos\left(\frac{m\pi}{L_x} x\right) \cos\left(\frac{n\pi}{L_y} y\right), \tag{34}$$

where E_{mn} is the coefficient of (m, n) mode of the energy density, and L_x and L_y are the dimensions of the plate as shown in Fig. 1. The input power can also be represented in the form of the cosine series:

$$\Pi_{in}\delta(x - x_o)\delta(y - y_o) = \sum_{m=0}^{\infty} \sum_{n=0}^{\infty} \Pi_{mn} \cos\left(\frac{m\pi}{L_x} x\right) \cos\left(\frac{n\pi}{L_y} y\right), \tag{35}$$

where the coefficient of (m, n) mode, Π_{mn}, is

$$\Pi_{mn} = \frac{\varepsilon_{mn}}{L_x L_y} \Pi_{in} \cos\left(\frac{m\pi}{L_x} x_0\right) \cos\left(\frac{n\pi}{L_y} y_0\right). \tag{36}$$

Here, the factor ε_{mn} is determined by

$$\varepsilon_{mn} = \begin{cases} 1, & m = 0 \text{ and } n = 0, \\ 2, & (m = 0 \text{ and } n \neq 0) \text{ or } (m \neq 0 \text{ and } n = 0), \\ 4, & m \neq 0 \text{ and } n \neq 0. \end{cases} \tag{37}$$

Substituting Eqs. (34) and (35) into the energy equation (30) yields the modal coefficient of the energy density solution in the following expression:

$$E_{mn} = \frac{\dfrac{\varepsilon_{mn}}{L_x L_y} \Pi_{in} \cos\left(\dfrac{m\pi}{L_x} x_o\right) \cos\left(\dfrac{n\pi}{L_y} y_o\right)}{\dfrac{c_{gx}^2}{\eta\omega}\left(\dfrac{m\pi}{L_x}\right)^2 + \dfrac{c_{gy}^2}{\eta\omega}\left(\dfrac{n\pi}{L_y}\right)^2 + \eta\omega}. \tag{38}$$

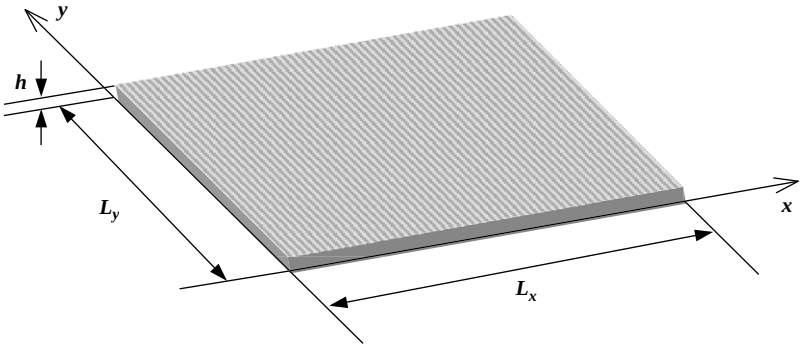

Fig. 1. Dimensions of the rectangular orthotropic plate.

The x and y components of the intensity can be obtained by substituting the energy density solution expressed by Eq. (34) into the energy transmission relation represented by Eqs. (24) and (25):

$$\langle \tilde{q}_x \rangle = \frac{c_{gx}^2}{\eta\omega} \sum_{m=1}^{\infty} \sum_{n=0}^{\infty} E_{mn} \left(\frac{m\pi}{L_x}\right) \sin\left(\frac{m\pi}{L_x}x\right) \cos\left(\frac{n\pi}{L_y}y\right) \tag{39}$$

and

$$\langle \tilde{q}_y \rangle = \frac{c_{gy}^2}{\eta\omega} \sum_{m=0}^{\infty} \sum_{n=1}^{\infty} E_{mn} \left(\frac{n\pi}{L_y}\right) \cos\left(\frac{m\pi}{L_x}x\right) \sin\left(\frac{n\pi}{L_y}y\right), \tag{40}$$

respectively.

3.2. Numerical examples

Numerical analyses are performed for the finite rectangular orthotropic plate simply supported along its edges and excited by a transverse harmonic point force as shown in Fig. 2. The time- and locally space-averaged energy density of farfield flexural waves is calculated by the approximate solution (Eq. (34)) of the energy equation developed in this work for vibrating orthotropic plates, and the intensity field in the plate is obtained from Eqs. (39) and (40). The energy density distributions obtained by the developed approximate power flow model are compared with the results obtained from the classical solution for the displacement of the corresponding plate (Appendix A). The dimensions and thickness of the plate shown in Fig. 1 are $L_x = L_y = 1$ m and $h = 1$ mm, respectively, and the material properties of the plate are assumed to be the same as those of pure aluminum. It is assumed that the plate is stiffened along the y direction and thus D_y is 20 times greater than D_x that is the bending stiffness of the original aluminum plate. The force is located at $x_0 = L_x/2$ and $y_0 = L_y/2$ in the plate and its amplitude is $F = 1$ N. The time-averaged input power can be calculated as follows:

$$\Pi_{in} = \frac{1}{2} \mathrm{Re}\left\{ \left(F e^{j\omega t}\right) \times \left(\frac{\partial w(x_0, y_0, t)}{\partial t}\right)^* \right\}, \tag{41}$$

where $w(x_0, y_0, t)$ can be obtained by Eq. (A.2) with $x = x_0$ and $y = y_0$. To obtain the PFA solutions, Eq. (41) is utilized as the input power Π_{in} included in Eq. (38).

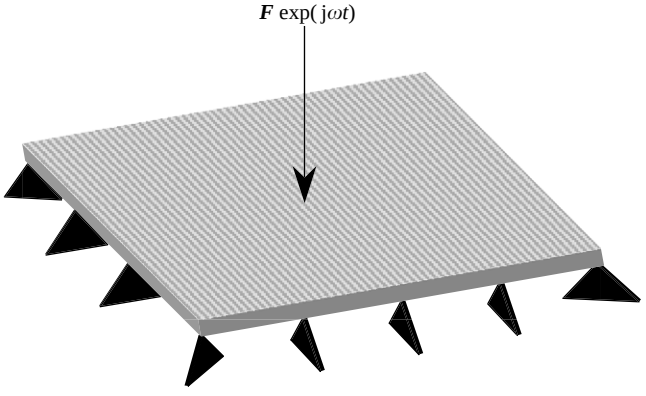

Fig. 2. Simple supports and external harmonic force on the plate.

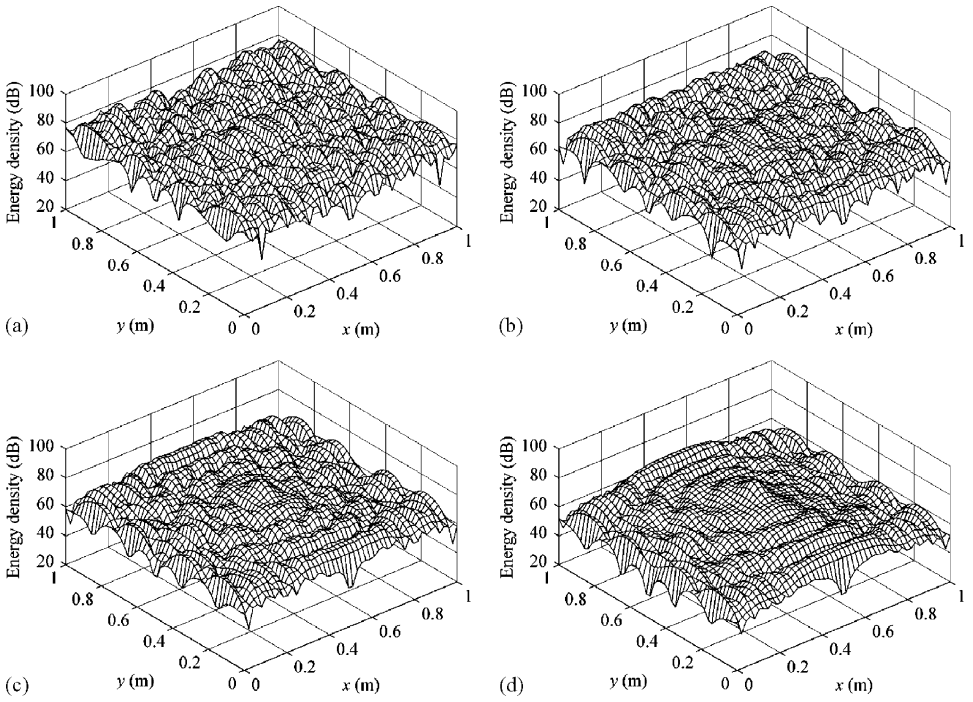

Fig. 3. Classical energy density distributions of the orthotropic plate when $f = 1\,\text{kHz}$, $x_0 = L_x/2$ and $y_0 = L_y/2$. The reference energy density is $1 \times 10^{-12}\ \text{J/m}^2$: (a) $\eta = 0.01$, (b) $\eta = 0.05$, (c) $\eta = 0.1$, (d) $\eta = 0.2$.

When the exciting frequency is $f = 1\,\text{kHz}$, the distributions of the energy density obtained from the classical displacement method (Eq. (4)) for various values of damping loss factor ($\eta = 0.01$, 0.05, 0.1 and 0.2) are shown in Fig. 3, and the corresponding results from the developed PFA model (Eq. (33)) are illustrated in Fig. 4. For the sufficient convergence of the solution, 90 000 lower modal terms of the Fourier series are accumulated to calculate the classical and PFA results, respectively. The reference energy density of the energy level is $1 \times 10^{-12}\ \text{J/m}^2$. As the plate is treated with larger damping, the global variation of the classical energy density becomes relatively faster as seen in Fig. 3. It can be observed in Fig. 4 that the PFA solutions represent well the global variation of the classical solutions, which may be used meaningfully for medium-to-high frequency problems. As the frequency of interest is increased, the uncertainties of the dynamic behavior become more prominent and the global phenomena come to give more significant information than the local phenomena.

When the frequency is set to be $f = 10\,\text{kHz}$, several patterns of energy density distribution predicted by the classical method can be observed in Fig. 5. In comparison with the previous case as shown in Fig. 3, the energy density decreases fast as going far from the excitation point. When the plate is treated with larger damping, the global variation of the result appears to be more obvious, which is well approximated by the PFA solutions as shown in Fig. 6. It should be noted that the energy density does not vary at the same rate for all directions due to the discrepancy between the values of the bending stiffnesses D_x and D_y, which can be easily observed with large damping as shown in Fig. 5(d), the corresponding global variation being well approximated by Fig. 6(d).

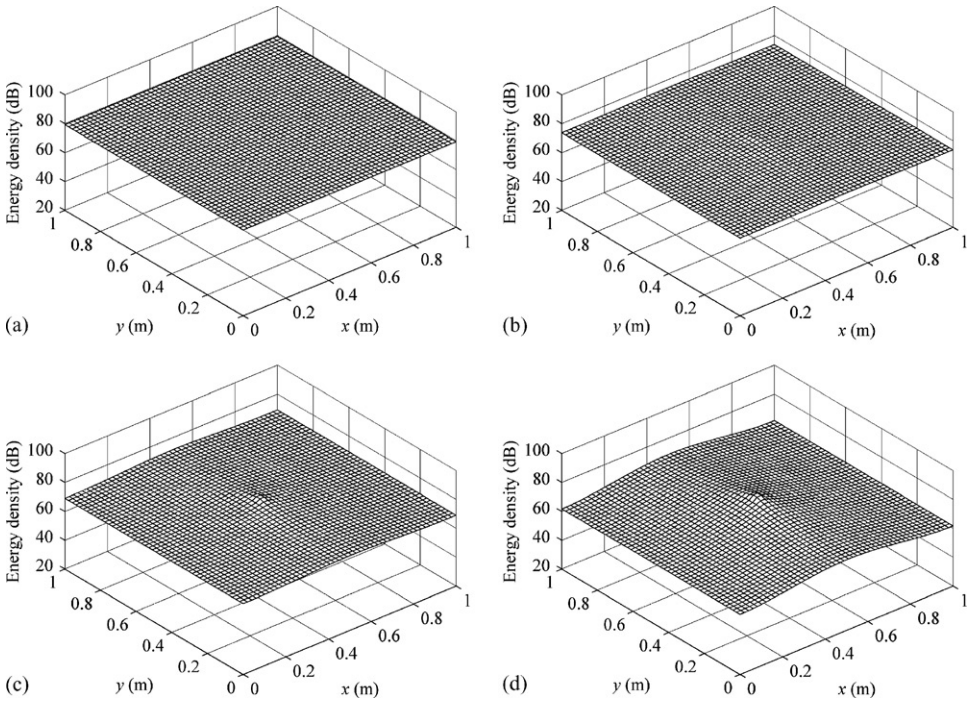

Fig. 4. Approximate energy density distributions of the orthotropic plate when $f = 1$ kHz, $x_0 = L_x/2$ and $y_0 = L_y/2$. The reference energy density is 1×10^{-12} J/m^2: (a) $\eta = 0.01$, (b) $\eta = 0.05$, (c) $\eta = 0.1$, (d) $\eta = 0.2$.

In Fig. 7, the energy density distributions predicted by the PFA model are compared with those by classical method along the line $x = L_x/2$. It can be found that the PFA solutions are useful in predicting the locally space-averaged distribution of the energy density. Fig. 8 illustrates the comparisons of the energy density distributions along the line $y = L_y/2$ in the plate, from which good agreements between the PFA solutions and the classical solutions are observed in the smoothed sense.

For the next examples, the energy levels of the classical and the PFA solutions are spatially averaged over the whole area of the plate, and are compared for different frequencies setting damping loss factors $\eta =$ at 0.01 and 0.1. For the spatial-averaging, 2500 points at regular intervals on the plate are used. It can be observed in Fig. 9 that the PFA energy levels are as a whole in good agreement with the classical energy levels.

The average energy levels of the classical and the PFA solutions are also plotted for various damping loss factors when the frequencies are set to be $f = 1$ kHz and 10 kHz. It can be seen in Fig. 10(a) that when the frequency is $f = 1$ kHz, two results are nearly constant up to about $\eta = 0.01$ and then begin to decrease smoothly as the damping is increased. In this frequency, the magnitudes of the error between the two kinds of the results are not over 1 dB for every damping loss factor of interest. If the frequency is increased to $f = 10$ kHz, the energy levels of two results are totally decreased and their errors also become negligible, as shown in Fig. 10(b).

In the last examples, the classical intensity fields and the approximate PFA intensity fields, when the frequency and the damping are $f = 1$ kHz and $\eta = 0.1$, are represented in Fig. 11. It can

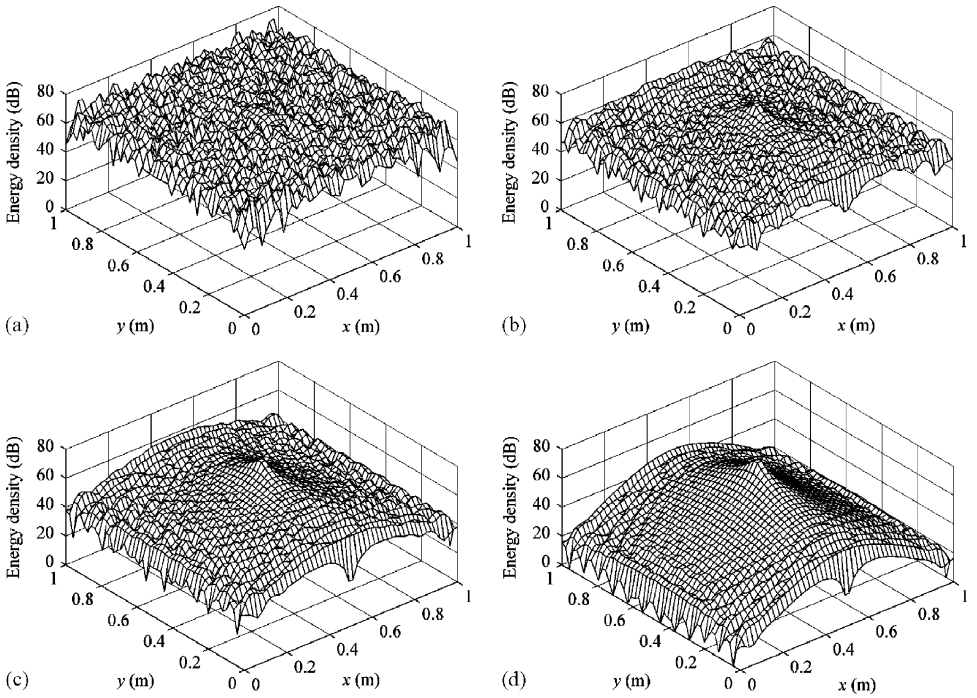

Fig. 5. Classical energy density distributions of the orthotropic plate when $f = 10\,\text{kHz}$, $x_0 = L_x/2$ and $y_0 = L_y/2$. The reference energy density is $1 \times 10^{-12}\,\text{J/m}^2$: (a) $\eta = 0.01$, (b) $\eta = 0.05$, (c) $\eta = 0.1$, (d) $\eta = 0.2$.

be known from the comparison of two results that the PFA solution is a good smoothed representation of the classical solution and may be usefully applied to predict the dominant power transmission paths. It can be seen in Fig. 12 that when the frequency is increased to $f = 10\,\text{kHz}$, the results of the both methods become more similar to each other.

4. Conclusions

An approximate power flow model for transversely vibrating orthotropic plates has been developed in order to extend the application range of the power flow analysis (PFA) method to the medium-to-high frequency vibration of orthotropic plate structures. To derive the corresponding energy equation, the farfield components of the plane wave were utilized, and time- and space-averaging were performed over a period and a half wavelength with the assumption that the damping is small. The developed model has a more general form covering the differences in the bending stiffness, and the PFA model of the isotropic plate can be easily derived as a specific case of the developed model. From numerical examples, the approximate energy and intensity field obtained by the derived energy equation are seen to well represent the global variation of the response with the reliable results.

Further studies on the development of new power flow models for in-plane waves of the orthotropic plate and on the prediction of the energy and intensity field in coupled orthotropic plates are recommended.

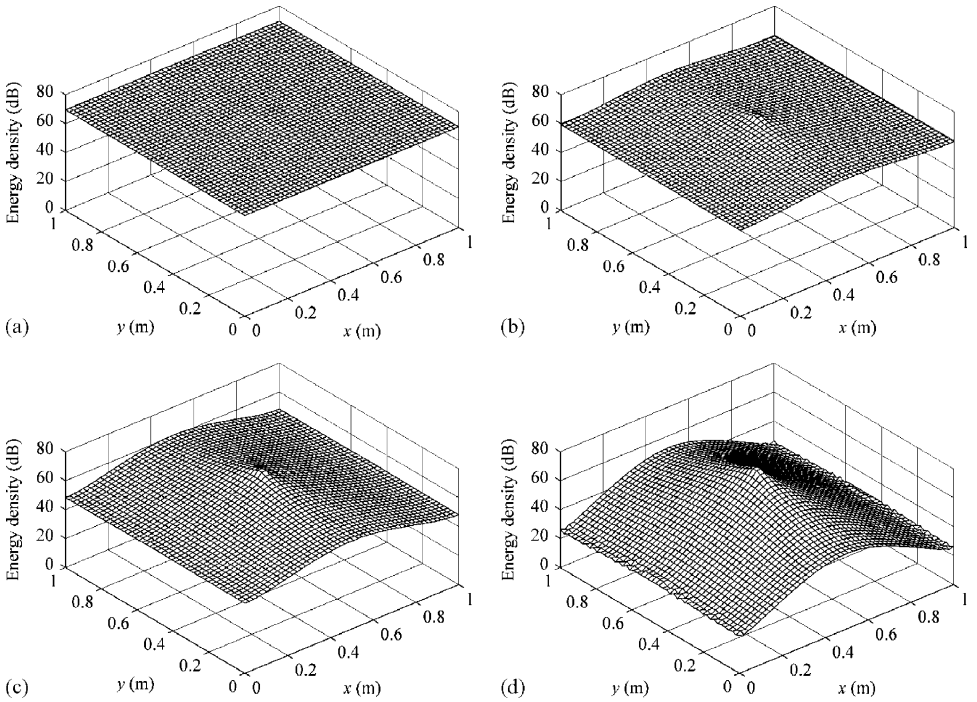

Fig. 6. Approximate energy density distributions of the orthotropic plate when $f = 10\,\text{kHz}$, $x_0 = L_x/2$ and $y_0 = L_y/2$. The reference energy density is $1 \times 10^{-12}\ \text{J/m}^2$: (a) $\eta = 0.01$, (b) $\eta = 0.05$, (c) $\eta = 0.1$, (d) $\eta = 0.2$.

Acknowledgements

This work was partially supported by Advanced Ship Engineering Research Center of the Korea Science & Foundation.

Appendix A. Classical solution

The equation of motion for an orthotropic plate excited by a harmonic point force may be given by

$$D_{xc}\frac{\partial^4 w}{\partial x^4} + 2\sqrt{D_{xc}D_{yc}}\,\frac{\partial^4 w}{\partial x^2 \partial y^2} + D_{yc}\frac{\partial^4 w}{\partial y^4} + m\frac{\partial^2 w}{\partial t^2} = F\delta(x - x_0)\delta(y - y_0)\mathrm{e}^{\mathrm{j}\omega t}. \tag{A.1}$$

When the plate is simply supported along its edges, the displacement solution of the equation of motion can be expressed by the double sine series of the spatial variables x and y:

$$w(x, y, t) = \sum_{m=1}^{\infty}\sum_{n=1}^{\infty} W_{mn}\,\sin\left(\frac{m\pi}{L_x}x\right)\sin\left(\frac{n\pi}{L_y}y\right)\exp(\mathrm{j}\omega t). \tag{A.2}$$

The force is also expressed by the double series of the sine function in the form:

$$F\delta(x - x_o)\delta(y - y_o)\exp(\mathrm{j}\omega t) = \sum_{m=1}^{\infty}\sum_{n=1}^{\infty} F_{mn}\sin\left(\frac{m\pi}{L_x}x\right)\sin\left(\frac{n\pi}{L_y}y\right)\exp(\mathrm{j}\omega t). \tag{A.3}$$

Substituting the displacement and force represented by the double series into the above equation of motion yields

$$W_{mn} = \frac{\frac{4}{L_x L_y} F \sin\left(\frac{m\pi}{L_x} x_0\right) \sin\left(\frac{n\pi}{L_y} y_0\right)}{D_{xc}\left(\frac{m\pi}{L_x}\right)^4 + 2\sqrt{D_{xc} D_{yc}}\left(\frac{m\pi}{L_x}\right)^2 \left(\frac{n\pi}{L_y}\right)^2 + D_{yc}\left(\frac{n\pi}{L_y}\right)^4 - \omega^2 m}. \tag{A.4}$$

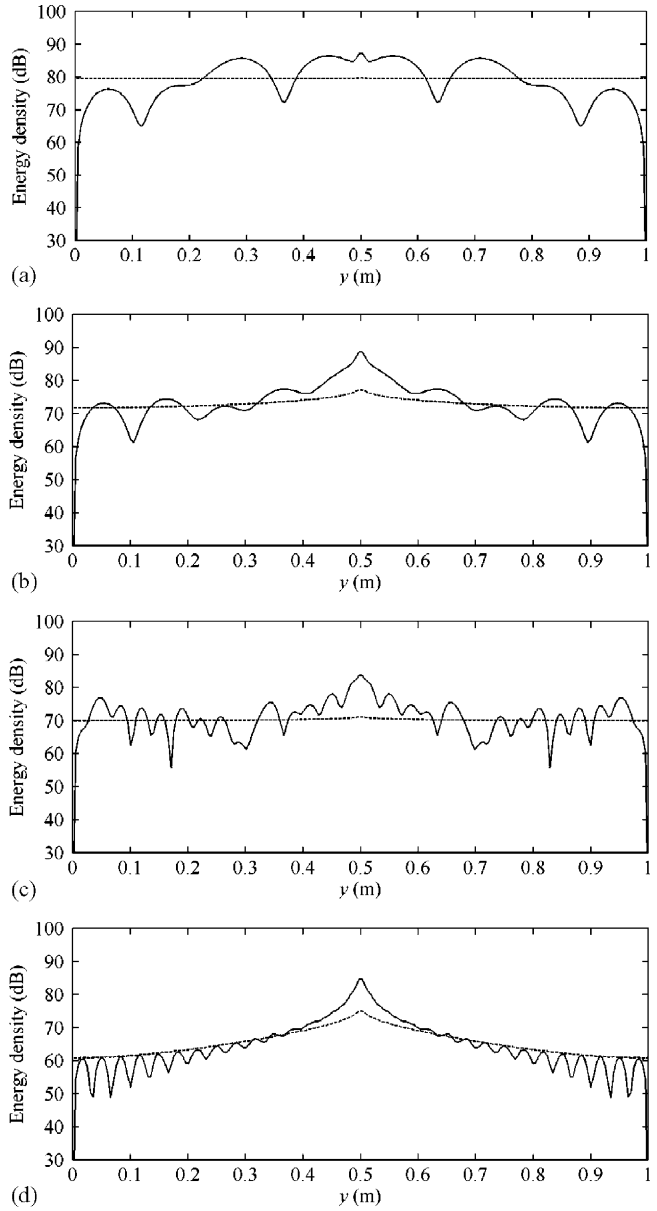

Fig. 7. Comparisons of the energy density distributions along the line $x = L_x/2$. The reference energy density is 1×10^{-12} J/m^2: (a) $f = 1$ kHz and $\eta = 0.01$, (b) $f = 1$ kHz and $\eta = 0.1$, (c) $f = 10$ kHz and $\eta = 0.01$, (d) $f = 10$ kHz and $\eta = 0.1$: — , classical solutions; ----, PFA solutions.

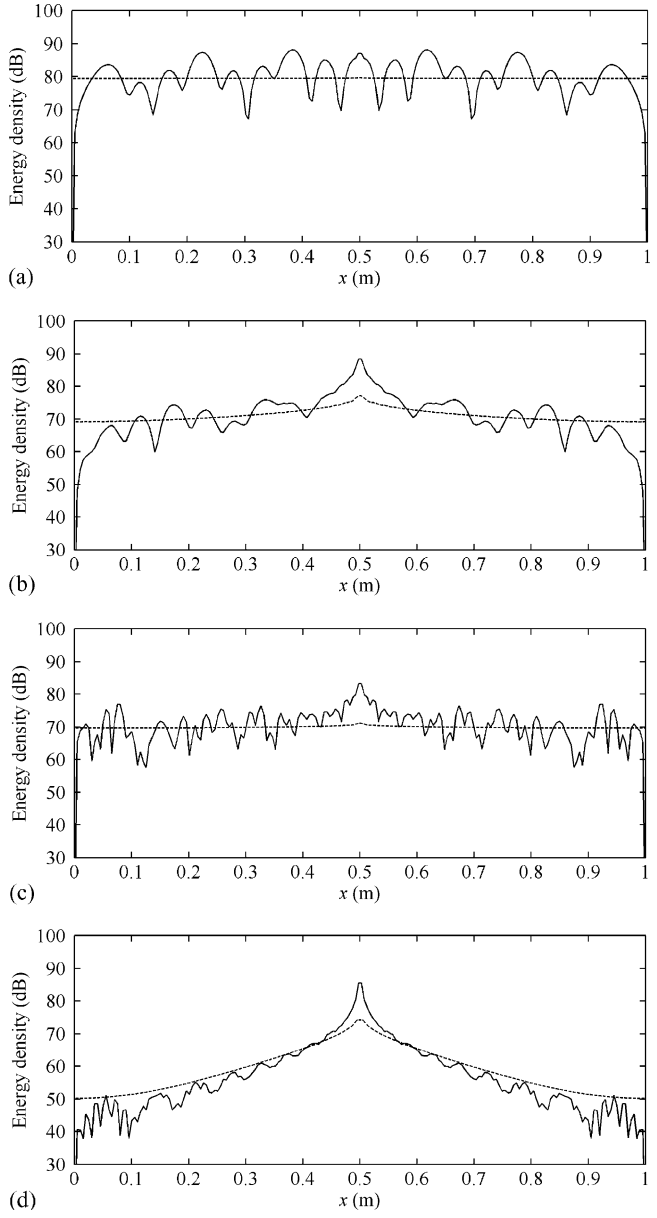

Fig. 8. Comparisons of the energy density distributions along the line $y = L_y/2$. The reference energy density is 1×10^{-12} J/m^2: (a) $f = 1$ kHz and $\eta = 0.01$, (b) $f = 1$ kHz and $\eta = 0.1$, (c) $f = 10$ kHz and $\eta = 0.01$, (d) $f = 10$ kHz and $\eta = 0.1$: — , classical solutions; ----, PFA solutions.

Thus, the displacement solution of the Eq. (A.1) can be obtained by substituting Eq. (A.4) into Eq. (A.2). After calculating the displacement solution, the time-averaged energy density can be finally calculated by substituting the obtained solution into Eq. (13). The x and y directional components of the time-averaged intensity can be also obtained by substituting the displacement solution into the Eqs. (14) and (15), respectively.

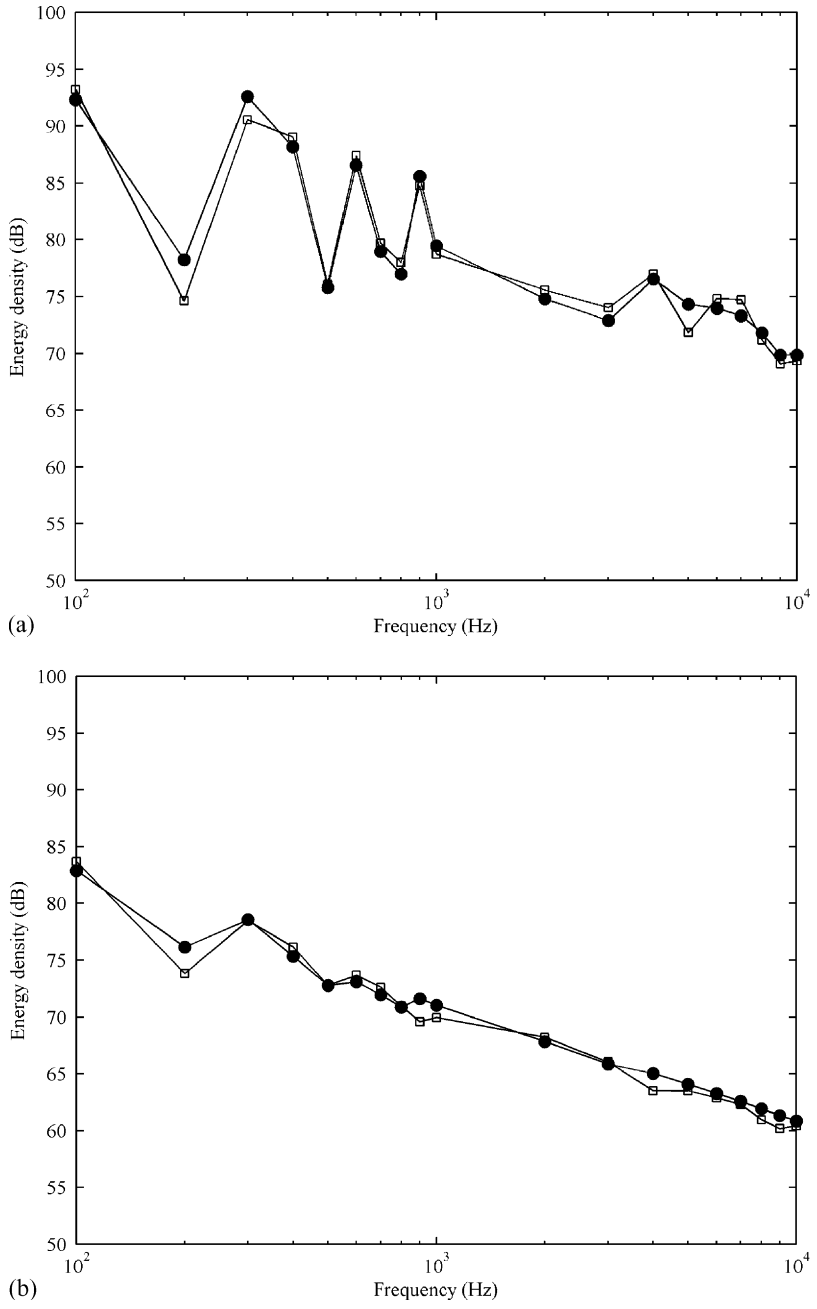

Fig. 9. Average energy levels of the orthotropic plate for various frequencies. The reference energy density is 1×10^{-12} J/m^2: (a) $\eta = 0.01$, (b) $\eta = 0.1$: —□—, classical solutions; —●—, PFA solutions.

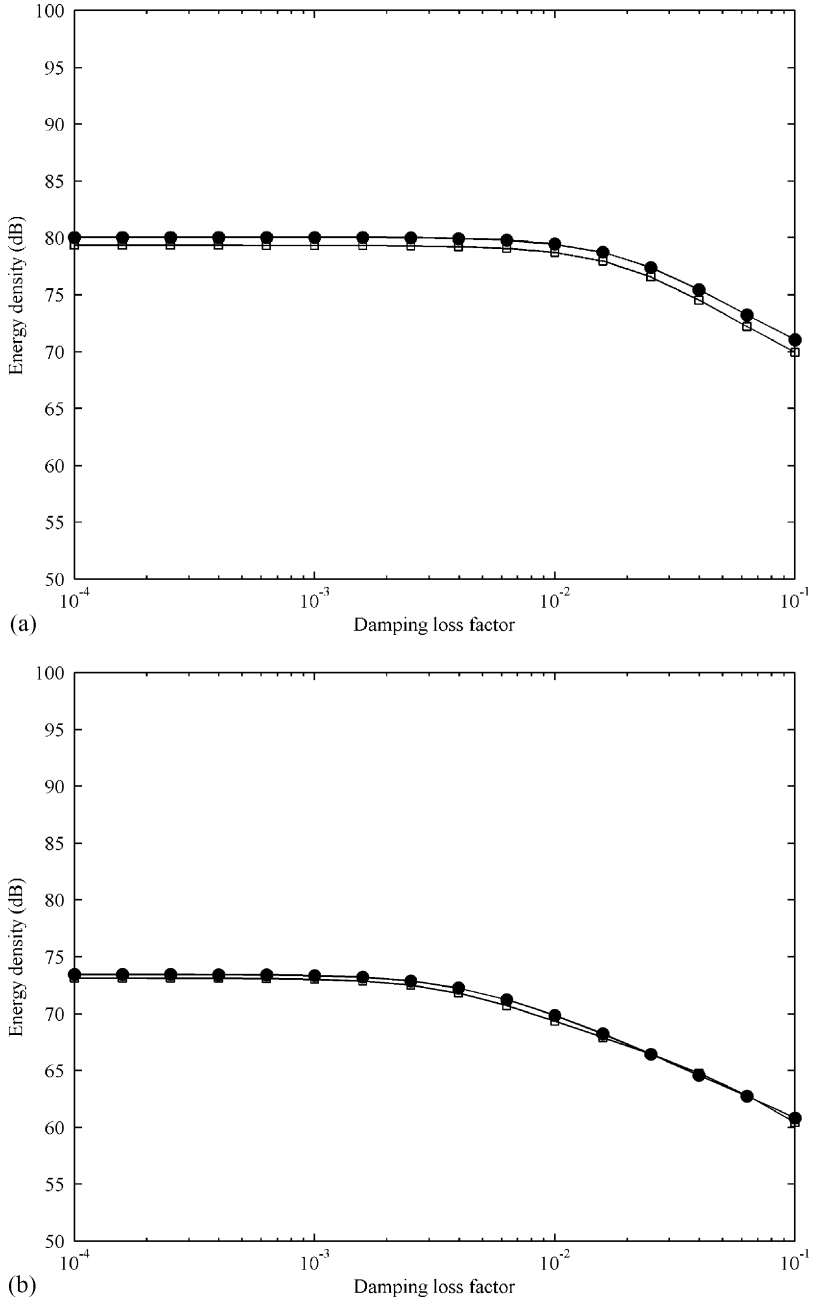

Fig. 10. Average energy levels of the orthotropic plate for various damping. The reference energy density is 1×10^{-12} J/m^2: (a) $f = 1$ kHz, (b) $f = 10$ kHz: —□—, classical solutions; —●—, PFA solutions.

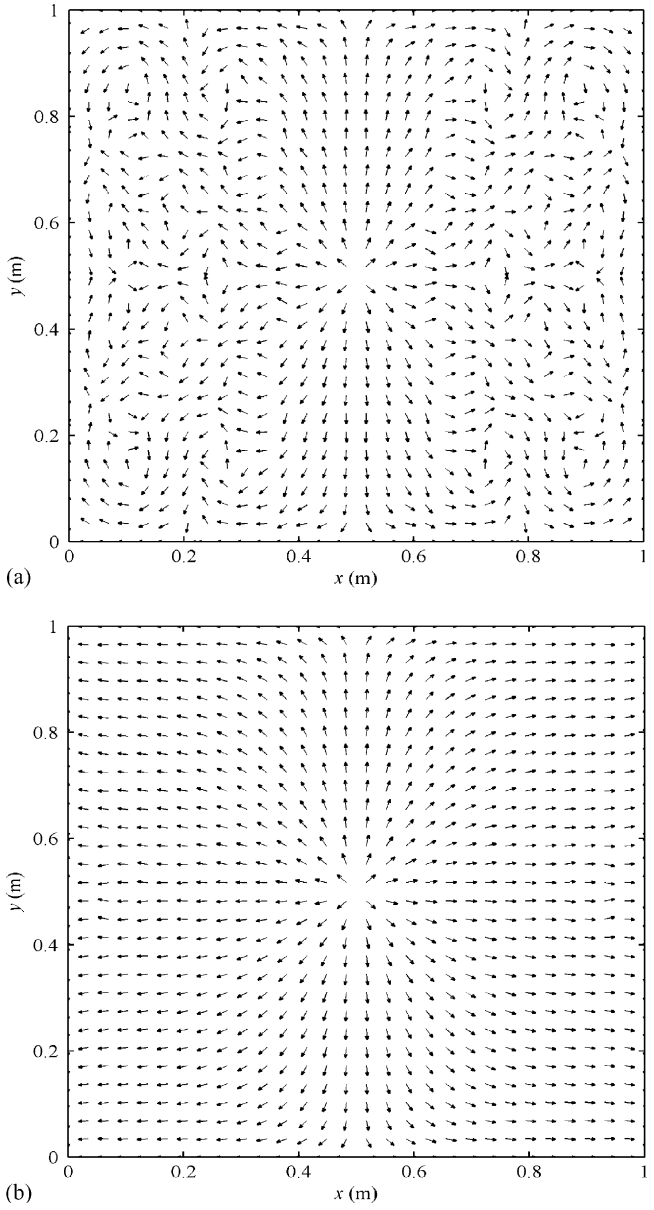

Fig. 11. Intensity distributions of the orthotropic plate when $f = 1\,\text{kHz}$, $\eta = 0.1$, $x_0 = L_x/2$ and $y_0 = L_y/2$. The reference intensity is $1 \times 10^{-12}\ \text{W/m}^2$: (a) classical solution, (b) PFA solution.

Appendix B. Space-averaging process

If Eq. (16) is expanded, the time-averaged total energy density can be rewritten as

$$\langle e \rangle = \langle e_1 \rangle + \langle e_2 \rangle, \tag{B.1}$$

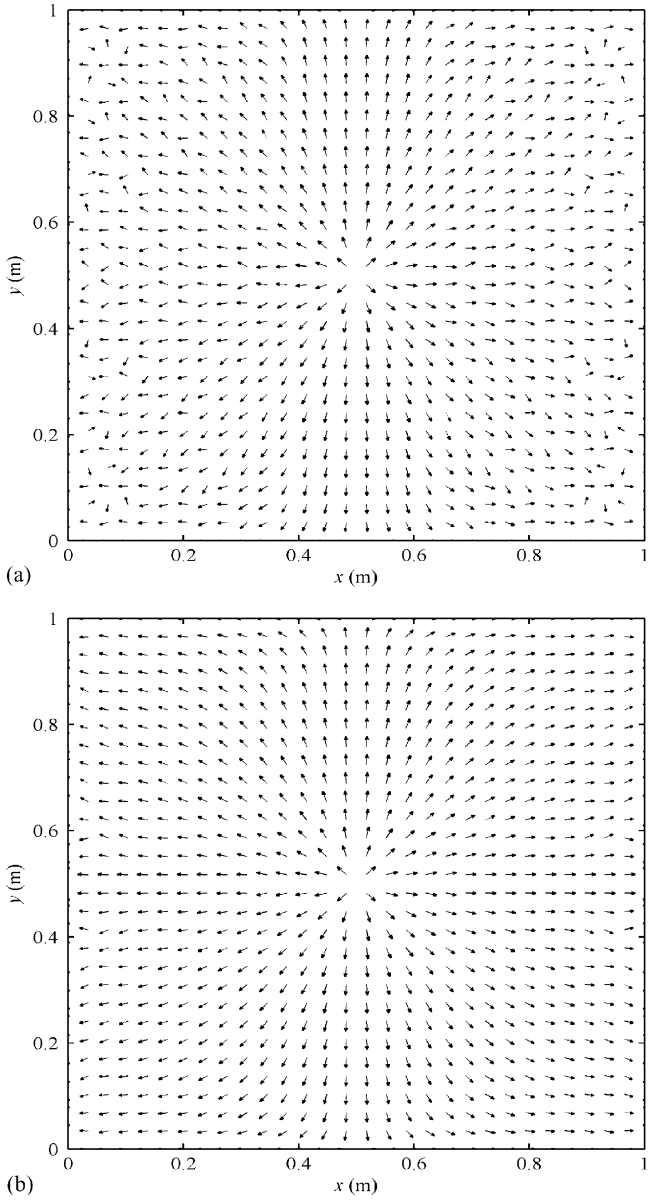

Fig. 12. Intensity distributions of the orthotropic plate when $f = 10\,\text{kHz}$, $\eta = 0.1$, $x_0 = L_x/2$ and $y_0 = L_y/2$. The reference intensity is $1 \times 10^{-12}\ \text{W/m}^2$: (a) classical solution, (b) PFA solution.

where $\langle e_1 \rangle$ and $\langle e_2 \rangle$ are defined here by

$$\langle e_1 \rangle = \tfrac{1}{4}\text{Re}\Big\{ \Big(D_{xc}|k_x|^4 + 2\sqrt{v_x v_y}\sqrt{D_{xc}D_{yc}}k_x^2 \Big(k_y^2\Big)^* + 2\Big(1 - \sqrt{v_x v_y}\Big)\sqrt{D_{xc}D_{yc}}|k_x|^2\big|k_y\big|^2 .. + D_{yc}\big|k_y\big|^4 + m\omega^2\Big)\Big(|[A]^{--}|^2 + \big|[B]^{+-}\big|^2 + \big|[C]^{-+}\big|^2 + \big|[D]^{++}\big|^2 \Big)\Big\} \tag{B.2}$$

and

$$\langle e_2\rangle = \tfrac{1}{4}\mathrm{Re}\Bigg\{\Bigg(D_{xc}|k_x|^4+2\sqrt{v_xv_y}\sqrt{D_{xc}D_{yc}}k_x^2\left(k_y^2\right)^*+2\left(1-\sqrt{v_xv_y}\right)\sqrt{D_{xc}D_{yc}}|k_x|^2|k_y|^2..$$
$$+D_{yc}|k_y|^4+m\omega^2\Bigg)\left([A]^{--}\left([B]^{+-}\right)^*+[B]^{+-}([A]^{--})^*+[A]^{--}\left([C]^{-+}\right)^*+[C]^{-+}([A]^{--})^*\right.$$
$$+[A]^{--}\left([D]^{++}\right)^*+[D]^{++}([A]^{--})^*+[B]^{+-}\left([C]^{-+}\right)^*+[C]^{-+}\left([B]^{+-}\right)^*+[B]^{+-}\left([D]^{++}\right)^*$$
$$\left.+[D]^{++}\left([B]^{+-}\right)^*+[C]^{-+}\left([D]^{++}\right)^*+[D]^{++}\left([C]^{-+}\right)^*\right)$$
$$-2\left(1-\sqrt{v_xv_y}\right)\sqrt{D_{xc}D_{yc}}|k_x|^2|k_y|^2\left([A]^{--}\left([B]^{+-}\right)^*+[B]^{+-}([A]^{--})^*+[A]^{--}\left([C]^{-+}\right)^*\right.$$
$$+[C]^{-+}([A]^{--})^*-[A]^{--}\left([D]^{++}\right)^*-[D]^{++}([A]^{--})^*-[B]^{+-}\left([C]^{-+}\right)^*-[C]^{-+}\left([B]^{+-}\right)^*$$
$$\left.+[D]^{++}\left([B]^{+-}\right)^*+[C]^{-+}\left([D]^{++}\right)^*+[D]^{++}\left([C]^{-+}\right)^*\right)\Bigg\}. \tag{B.3}$$

Substituting Eq. (B.1) into Eq. (19) yields the time- and locally space-averaged total energy density:

$$\langle\tilde{e}\rangle = \frac{k_{xl}k_{yl}}{\pi^2}\int_0^{\pi/k_{yl}}\int_0^{\pi/k_{xl}}\langle e_1\rangle+\langle e_2\rangle\,\mathrm{d}x\,\mathrm{d}y = \langle\tilde{e}_1\rangle+\langle\tilde{e}_2\rangle. \tag{B.4}$$

Then, the integrals for the first unknown term $|[A]^{--}|^2$ in Eq. (B.2) become

$$\int_0^{\pi/k_{yl}}\int_0^{\pi/k_{xl}}|[A]^{--}|^2\mathrm{d}x\,\mathrm{d}y = \int_0^{\pi/k_{yl}}\int_0^{\pi/k_{xl}}|A|^2\mathrm{e}^{-(\eta/2)k_{xl}x-(\eta/2)k_{yl}y}\mathrm{d}x\,\mathrm{d}y \tag{B.5}$$

where if the damping of the plate is small ($\eta\ll 1$), the exponential function in the right-hand side can be assumed to be nearly constant on the intervals of integration $0\leqslant x\leqslant(\pi/k_{xl})$ and $0\leqslant y\leqslant(\pi/k_{yl})$:

$$\int_0^{\pi/k_{yl}}\int_0^{\pi/k_{xl}}|A|^2\mathrm{e}^{-(\eta/2)k_{xl}x-(\eta/2)k_{yl}y}\mathrm{d}x\,\mathrm{d}y\approx|A|^2e^{--}\int_0^{\pi/k_{yl}}\int_0^{\pi/k_{xl}}\mathrm{d}x\,\mathrm{d}y$$
$$=\frac{\pi^2}{k_{xl}k_{yl}}|A|^2e^{--}. \tag{B.6}$$

The other unknown terms in Eq. (B.2) can be also integrated through the same process. Consequently, $\langle\tilde{e}_1\rangle$ can be obtained by

$$\langle\tilde{e}_1\rangle = \tfrac{1}{4}\mathrm{Re}\Bigg\{D_{xc}|k_x|^4+2\sqrt{v_xv_y}\sqrt{D_{xc}D_{yc}}k_x^2\left(k_y^2\right)^*+2\left(1-\sqrt{v_xv_y}\right)\sqrt{D_{xc}D_{yc}}|k_x|^2|k_y|^2.$$
$$+D_{yc}|k_y|^4+m\omega^2\Bigg\}\left(|A|^2e^{--}+|B|^2e^{+-}+|C|^2e^{-+}+|D|^2e^{++}\right). \tag{B.7}$$

The integrals for the first unknown term $[A]^{--}([B]^{+-})^*$ in Eq. (B.3) can be obtained in the similar way:

$$\int_0^{\pi/k_{yl}}\int_0^{\pi/k_{xl}}[A]^{--}\left([B]^{+-}\right)^*\mathrm{d}x\mathrm{d}y = AB^*\int_0^{\pi/k_{yl}}\mathrm{e}^{-(\eta/2)k_{yl}y}\int_0^{\pi/k_{xl}}\mathrm{e}^{-2jk_{xl}x}\mathrm{d}x\mathrm{d}y$$
$$= AB^*\int_0^{\pi/k_{yl}}\mathrm{e}^{-(\eta/2)k_{yl}y}\frac{\mathrm{e}^{-2jk_{xl}x}}{-2jk_{xl}}\bigg|_{x=0}^{x=\pi/k_{xl}}\mathrm{d}y = 0 \tag{B.8}$$

As seen in Eq. (B.8), all of the other unknown terms come to be zero due to the integration. Thus, $\langle\tilde{e}_2\rangle$ is nullified:

$$\langle\tilde{e}_2\rangle = 0, \tag{B.9}$$

from which the time- and locally space-averaged total energy density $\langle\tilde{e}\rangle$ comes to be equal to $\langle\tilde{e}_1\rangle$:

$$\langle\tilde{e}\rangle = \langle\tilde{e}_1\rangle. \tag{B.10}$$

When the coefficient terms, Re{....}, in Eq. (B.8) are considered, they include high order terms of damping loss factor η as follows:

$$\mathrm{Re}\left\{D_{xc}|k_x|^4+2\sqrt{v_xv_y}\sqrt{D_{xc}D_{yc}}k_x^2\left(k_y^2\right)^*+2\left(1-\sqrt{v_xv_y}\right)\sqrt{D_{xc}D_{yc}}|k_x|^2|k_y|^2+D_{yc}|k_y|^4+m\omega^2\right\}$$
$$= \left|1-j\frac{\eta}{4}\right|^4\left(D_xk_{xl}^4+2\sqrt{v_xv_y}\sqrt{D_xD_y}k_{xl}^2k_{yl}^2+2\left(1-\sqrt{v_xv_y}\right)\sqrt{D_xD_y}k_{xl}^2k_{yl}^2+D_yk_{yl}^4\right)+m\omega^2$$
$$= \left(1+\frac{\eta^2}{8}+\frac{\eta^4}{256}\right)\left(\sqrt{D_x}k_{xl}^2+\sqrt{D_y}k_{yl}^2\right)^2+m\omega^2. \tag{B.11}$$

Neglecting all of the second and higher order terms of the damping loss factor and substituting the dispersion relation (Eq. (6)) into Eq. (B.11), the time- and locally space-averaged total energy density $\langle\tilde{e}\rangle$ can be finally obtained as the simplified Eq. (21).

When spatially averaging the intensity (Eqs. (17) and (18)) over a half wavelength, one can obtain the following expressions through the same process of Eqs. (B.6) and (B.8):

$$\langle\tilde{q}_x\rangle = \frac{\omega}{2}\,\mathrm{Re}\left\{k_x\left(D_{xc}k_x^2+\sqrt{D_{xc}D_{yc}}k_y^2\right)+D_{xc}\left(k_x^2+v_yk_y^2\right)k_x^*\right.$$
$$\left.+\left(1-\sqrt{v_xv_y}\right)\sqrt{D_{xc}D_{yc}}k_x|k_y|^2\right\}\left(|A|^2\mathrm{e}^{--}-|B|^2\mathrm{e}^{+-}+|C|^2\mathrm{e}^{-+}-|D|^2\mathrm{e}^{++}\right) \tag{B.12}$$

and

$$\tilde{q}_y = \frac{\omega}{2}\mathrm{Re}\left\{k_y\left(D_{yc}k_y^2+\sqrt{D_{xc}D_{yc}}k_x^2\right)+D_{yc}\left(k_y^2+v_xk_x^2\right)k_y^*\right.$$
$$\left.+\left(1-\sqrt{v_xv_y}\right)\sqrt{D_{xc}D_{yc}}k_y|k_x|^2\right\}\left(|A|^2\mathrm{e}^{--}+|B|^2\mathrm{e}^{+-}-|C|^2\mathrm{e}^{-+}-|D|^2\mathrm{e}^{++}\right). \tag{B.13}$$

The coefficient terms in Eq. (B.12) have high order terms of damping loss factor that is assumed to be small:

$$\begin{aligned}&\mathrm{Re}\left\{k_x\left(D_{xc}k_x^2+\sqrt{D_{xc}D_{yc}}k_y^2\right)+D_{xc}\left(k_x^2+v_yk_y^2\right)k_x^*+\left(1-\sqrt{v_xv_y}\right)\sqrt{D_{xc}D_{yc}}k_x|k_y|^2\right\}\\&=\left(1-\frac{\eta^2}{16}+\frac{\eta^4}{64}\right)k_{xl}\left(D_xk_{xl}^2+\sqrt{D_xD_y}k_{yl}^2\right)+\left(1+\frac{7}{16}\eta^2-\frac{\eta^4}{64}\right)D_x\left(k_{xl}^2+v_yk_{yl}^2\right)k_{xl}\\&\quad+\left(1+\frac{5}{16}\eta^2+\frac{\eta^4}{64}\right)k_{xl}\left(1-\sqrt{v_xv_y}\right)\sqrt{D_xD_y}k_{yl}^2.\end{aligned}\tag{B.14}$$

The coefficient terms in Eq. (B.13) can be written by

$$\begin{aligned}&\mathrm{Re}\left\{k_y\left(D_{yc}k_y^2+\sqrt{D_{xc}D_{yc}}k_x^2\right)+D_{yc}\left(k_y^2+v_xk_x^2\right)k_y^*+\left(1-\sqrt{v_xv_y}\right)\sqrt{D_{xc}D_{yc}}k_y|k_x|^2\right\}\\&=\left(1-\frac{\eta^2}{16}+\frac{\eta^4}{64}\right)k_{yl}\left(D_yk_{yl}^2+\sqrt{D_xD_y}k_{xl}^2\right)+\left(1+\frac{7}{16}\eta^2-\frac{\eta^4}{64}\right)D_y\left(k_{yl}^2+v_xk_{xl}^2\right)k_{yl}\\&\quad+\left(1+\frac{5}{16}\eta^2+\frac{\eta^4}{64}\right)k_{yl}\left(1-\sqrt{v_xv_y}\right)\sqrt{D_xD_y}k_{xl}^2.\end{aligned}\tag{B.15}$$

Here, neglecting all of the second and higher order terms of the damping loss factor and substituting the dispersion relation (Eq. (6)) and Betti's reciprocity ($v_xD_y = v_yD_x$) into Eqs. (B.14) and (B.15), the time- and locally space-averaged intensity components can be finally obtained as the simplified Eqs. (22) and (23).

References

[1] V.D. Belov, S.A. Rybak, B.D. Tartakovskii, Propagation of vibrational energy in absorbing structures, Soviet-Physics Acoustics 23 (1977) 115–119.
[2] D.J. Nefske, S.H. Sung, Power flow finite element analysis of dynamic systems: basic theory and application to beams, Journal of Vibration, Acoustics, Stress and Reliability in Design 111 (1989) 94–100.
[3] J.C. Wohlever, R.J. Bernhard, Mechanical energy flow models of rods and beams, Journal of Sound and Vibration 153 (1992) 1–19.
[4] O.M. Bouthier, R.J. Bernhard, C. Wohlever, Energy and structural intensity formulations of beam and plate vibrations, Proceedings of the 3rd International Congress on Intensity Techniques, Senlis, France, 1990, pp. 37–44.
[5] P.E. Cho, Energy Flow Analysis of Coupled Structures, Ph.D. Dissertation, Purdue University, 1993.
[6] O.M. Bouthier, R.J. Bernhard, Models of space-averaged energetics of plates, American Institute of Aeronautics and Astronautics Journal 30 (1992) 616–623.
[7] O.M. Bouthier, R.J. Bernhard, Simple models of the energetics of transversely vibrating plates, Journal of Sound and Vibration 182 (1995) 149–164.
[8] D.-H. Park, S.-Y. Hong, H.-G. Kil, J.-J. Jeon, Power flow models and analysis of in-plane waves in finite coupled thin plates, Journal of Sound and Vibration 244 (2001) 651–668.
[9] M.S. Troitsky, Stiffened Plates; Bending, Stability and Vibrations, Elsevier, Amsterdam, 1976.
[10] R. Szilard, Theory and Analysis of Plates; Classical and Numerical Methods, Prentice-Hall, Englewood Cliffs, NJ, 1974.
[11] S.A. Ambartsumyan, Theory of Anisotropic Plates; Strength, Stability and Vibrations, Hemisphere, New York, 1991.
[12] L. Cremer, M. Heckl, E.E. Ungar, Structure-Borne Sound, Springer, Berlin, 1973.
[13] D.U. Noiseux, Measurement of power flow in uniform beams and plates, Journal of the Acoustical Society of America 47 (1970) 238–247.
[14] S. Timoshenko, W. Woinowski-Krieger, Theory of Plates and Shells, McGraw-Hill, New York, 1959.